



Chinese Pharmaceutical Association
Institute of Materia Medica, Chinese Academy of Medical Sciences

Acta Pharmaceutica Sinica B

www.elsevier.com/locate/apsb
www.sciencedirect.com



ORIGINAL ARTICLE

Repurposing lansoprazole to alleviate metabolic syndrome *via* PHOSPHO1 inhibition



Yingting Wu^a, Jiaqi Xin^b, Xinyu Li^a, Ting Yang^a, Yi Liu^a,
Yongsheng Zhao^a, Wen Xie^{c,*}, Mengxi Jiang^{a,d,*}

^aDepartment of Pharmacology, School of Basic Medical Sciences, Capital Medical University, Beijing 100069, China

^bDepartment of Traditional Chinese Medicine, Capital Medical University, Beijing 100069, China

^cCenter for Pharmacogenetics and Department of Pharmaceutical Sciences, University of Pittsburgh, Pittsburgh, PA 15261, USA

^dAdvanced Innovation Center for Human Brain Protection, Capital Medical University, Beijing 100069, China

Received 12 August 2023; received in revised form 24 October 2023; accepted 6 December 2023

KEY WORDS

Lansoprazole;
Proton pump inhibitors;
Adipose thermogenesis;
Energy expenditure;
Metabolic syndrome;
PHOSPHO1 inhibitor;
Cannabinoid receptor
signaling;
Drug repurposing

Abstract Drug repurposing offers an efficient approach to therapeutic development. In this study, our bioinformatic analysis first predicted an association between obesity and lansoprazole (LPZ), a commonly prescribed drug for gastrointestinal ulcers. We went on to show that LPZ treatment increased energy expenditure and alleviated the high-fat diet-induced obesity, insulin resistance, and hepatic steatosis in mice. Treatment with LPZ elicited thermogenic gene expression and mitochondrial respiration in primary adipocytes, and induced cold tolerance in cold-exposed mice, suggesting the activity of LPZ in promoting adipose thermogenesis and energy metabolism. Mechanistically, LPZ is an efficient inhibitor of adipose phosphocholine phosphatase 1 (PHOSPHO1) and produces metabolic benefits in a PHOSPHO1-dependent manner. Our results suggested that LPZ may stimulate adipose thermogenesis by inhibiting the conversion of 2-arachidonoylglycerol-lysophosphatidic acid (2-AG-LPA) to 2-arachidonoylglycerol (2-AG) and reduce the activity of the thermogenic-suppressive cannabinoid receptor signaling. In summary, we have uncovered a novel therapeutic indication and mechanism of LPZ in managing obesity and its related metabolic syndrome, and identified a potential metabolic basis by which LPZ improves energy metabolism.

© 2024 The Authors. Published by Elsevier B.V. on behalf of Chinese Pharmaceutical Association and Institute of Materia Medica, Chinese Academy of Medical Sciences. This is an open access article under the CC BY-NC-ND license (<http://creativecommons.org/licenses/by-nc-nd/4.0/>).

*Corresponding authors.

E-mail addresses: jmx@ccmu.edu.cn (Mengxi Jiang), wex6@pitt.edu (Wen Xie).

Peer review under the responsibility of Chinese Pharmaceutical Association and Institute of Materia Medica, Chinese Academy of Medical Sciences.

<https://doi.org/10.1016/j.apsb.2024.01.001>

2211-3835 © 2024 The Authors. Published by Elsevier B.V. on behalf of Chinese Pharmaceutical Association and Institute of Materia Medica, Chinese Academy of Medical Sciences. This is an open access article under the CC BY-NC-ND license (<http://creativecommons.org/licenses/by-nc-nd/4.0/>).

1. Introduction

The rising global incidence of obesity and its related comorbidities, including type 2 diabetes, cardiovascular disease, and cancer, leads to a mounting socioeconomic and medical burden and poses a significant public health concern¹. Despite lifestyle intervention being a recommended strategy, achieving consistent and effective weight loss in obese patients remains challenging. Furthermore, current treatments such as bariatric surgery and pharmacotherapy are limited by their associated contraindications, complications, and adverse effects^{2,3}. Adipose thermogenesis consumes a substantial amount of energy and can be utilized to work against weight gain. While cold exposure and activation of β -adrenergic signaling can trigger adipose thermogenesis⁴, they are not practical treatments for obesity due to their demanding regimens and potential systemic toxicities⁵. Therefore, there is a vital need to gain an in-depth understanding of adipose thermogenesis and obesity pathology to identify novel and practical therapeutic targets and agents for treating obesity and its comorbidities.

Drug repurposing presents an efficient strategy to identify novel therapeutic indications due to a shortened drug development timeline, cost-effectiveness, and comprehensive safety profiles. In this study, we identified an association between proton pump inhibitors (PPIs) and obesity development through bioinformatic analysis, based on which we repurposed lansoprazole, a well-known PPI used to treat gastrointestinal ulcers, to stimulate adipose thermogenesis and mitigate obesity and insulin resistance in mouse models, which underscores the therapeutic potential of repurposing existing medications to address obesity-related metabolic disorders.

2. Materials and methods

2.1. Animals

C57BL/6J male mice (20–25 g) were purchased from Vital River Laboratories and housed in a specific pathogen-free (SPF) grade animal facility of Capital Medical University. *Phosphol*^{-/-} mice were a gift from Professor Colin Farquharson of the University of Edinburgh⁶ and were maintained on C57BL/6J background in the SPF animal facility of Capital Medical University. All animal experiments were performed under the Guidelines for Animal Care and Use to Medical Research approved by Capital Medical University (protocol number: AEEI-2019-119). Mice were closely monitored for postural alterations and behavioral changes to ensure that animal suffering was minimized throughout all aspects of experimentation.

2.2. Cold exposure and drug treatment

LPZ (Yuanye Bio-Technology) was dissolved in saline containing 1% DMSO (vehicle solution). Mice maintained at 20 °C were pretreated with vehicle or LPZ (10 mg/kg) by subcutaneous injection for one week before being transferred to 4 °C for acute cold exposure. The dose of LPZ used in this study was determined based on the clinically relevant dose and the body surface area conversion factor between mice and human^{7,8}. The rectal core body temperature of mice was measured by a UT323 microprobe thermometer (Uni-Trend Technology). The BAT and tail temperature were measured by the infrared camera detection system (FOTRIC) and analyzed by AnalyzIR software (version 4.3.1.15).

2.3. High-fat diet (HFD) treatment, body composition analysis, and indirect calorimetry

The mice were fed with HFD (MP Biomedicals) containing 60 kcal% calorie value, which was replaced every three days and weighted to calculate food intake. When necessary, mice were subcutaneously injected with either vehicle or LPZ (10 mg/kg) daily until the completion of the experiments, when serum, different adipose depots and liver samples were dissected and weighted for subsequent analysis. The bone and fat volume of mice was recorded using the SKyScan micro-CT scanner (Bruker). Volumetric micro-CT data were post-processed *via* Gaussian smoothing, and analyzed using the CTAn software (Bruker), wherein regions of interest were manually delineated. Energy expenditure was measured by the Promethion calorimetry system (Sable Systems International).

2.4. Glucose tolerance test (GTT) and insulin tolerance test (ITT)

GTT was performed in 16 h fasted mice by intraperitoneally injecting with glucose (2 g/kg). ITT was performed in 6 h fasted mice by intraperitoneally injecting with insulin (0.5 U/kg). Blood glucose was measured from the tail vein by the Contour TS meter (Ascensia Diabetes Care Holdings AG) every 0.5 h.

2.5. Measurement of serum insulin

Serum levels of insulin from HFD-fed mice were measured using the Ultra-Sensitive Mouse Insulin ELISA Kit (Crystal Chem) following the provided manufacturer's instructions.

2.6. Histology and quantification of adipocyte size

Freshly dissected tissues were fixed in 4% formaldehyde (Servicebio) overnight and replaced with 70% ethanol before paraffin embedding and tissue sections. The slides were stained with hematoxylin and eosin (H&E) and imaged by Axioscope A1 microscope and Zen lite software (Carl Zeiss Microscopy GmbH). To quantify adipocyte sizes, digital images of H&E staining sections were analyzed by the Adiposoft Plugin of the ImageJ software (version 1.53q, National Institutes of Health).

2.7. Cell culture and measurement of oxygen consumption rate

Differentiation of primary mouse adipocytes was described previously⁹ using reagents shown in [Supporting Information Table S1](#). Briefly, adipose tissues (BAT and iWAT) were dissected from 2–4-week-old male C57BL/6J mice bred in-house and digested with HBSS (Servicebio) containing 0.2% collagenase A (Roche) and 2% bovine serum albumin (Servicebio) at 37 °C for 30 min. The stromal vascular fraction was then isolated by centrifugation at 700×g (5804 R, Eppendorf, Hamburg, Germany) for 5 min and cultured in DMEM/F12 with 10% fetal bovine serum (FBS) prior to differentiation. Human adipose-derived mesenchymal stem cells (OriCell) were cultured in DMEM with 10% FBS and 100 U/mL penicillin/streptomycin (Servicebio) until reaching confluence, when cells were differentiated and replenished with differentiation medium every 3 days as shown in [Supporting Information Table S2](#)¹⁰. After 9–12 days of differentiation induction, cells were fed with the maintenance medium until fully differentiated.

When necessary, differentiated mature adipocytes were treated with 10 $\mu\text{mol/L}$ LPZ, 0.1 $\mu\text{mol/L}$ 2-arachidonoylglycerol (MedChemExpress), 0.1 $\mu\text{mol/L}$ choline (Tan-Mo Technology), 20 $\mu\text{mol/L}$ rimonabant (Yuanye Bio-Technology), 10 $\mu\text{mol/L}$ lansoprazole sulfone (MedChemExpress), 10 $\mu\text{mol/L}$ 5-hydroxylansoprazole (MedChemExpress), or 10 $\mu\text{mol/L}$ esomeprazole sodium (Yuanye Bio-Technology).

Seahorse assay was performed as described previously⁹. Briefly, primary adipocytes were seeded in 0.5% gelatin-coated 96-well Seahorse plates and assayed with 0.5–1 $\mu\text{mol/L}$ oligomycin, 1 $\mu\text{mol/L}$ FCCP, 0.5 $\mu\text{mol/L}$ rotenone and 0.5 $\mu\text{mol/L}$ antimycin A using Seahorse XF-96 Extracellular Flux Analyzer (Agilent Technologies). The cellular mitochondrial respiratory activities were analyzed by the Wave software (version 2.6.3.5, Agilent Technologies).

2.8. Untargeted metabolomics

30 mg of accurately weighted BAT or iWAT were homogenized in 200 μL of methanol:water (3:1) mixture under cold conditions. The tissue homogenates were vortexed for 10 min at 4 °C and centrifuged at 13,000 rpm (Heraeus Fresco 21, Thermo Fisher Scientific, Hamburg, Germany) for 15 min at 4 °C. The supernatant was carefully collected and dried under nitrogen gas, resuspended with 100 μL of acetonitrile and centrifuged at 13,000 rpm for 10 min at 4 °C before UPLC–QTOF–MS/MS analysis at the pharmaceutical core facility of Capital Medical University. The chromatographic separation of different metabolites was performed on an Acclaim RSLC C18 column (ThermoFisher Scientific). Mass spectrometry analysis was conducted using the SYNAPT G2-Si high-definition mass spectrometer (Waters) equipped with an electrospray ionization source. The acquired data were imported into Progenesis QI software for data normalization using peak alignment and baseline correction. The processed data were then searched against compound databases (KEGG, HMDB) using ChemSpider to obtain accurate molecular weight and fragmentation information of the compounds. Differentially enriched metabolites ($P < 0.05$, fold change > 1.2 , variable importance in projection score > 1 , and those including mass spectrometry fragments) were selected.

2.9. Quantitation of Cho and ChoP by UPLC–MS/MS

20 μL of serum samples or trypsinized mature adipocytes were mixed with 60 μL of methanol containing the internal standard. Samples were vortexed at 4 °C for 15 min and centrifuged at 13,000 rpm at 4 °C for 15 min. The supernatants were separated and diluted for quantitation analysis. 30 mg of BAT or iWAT samples were homogenized in 200 μL of methanol–water (3:1) mixtures and centrifuged. 20 μL of supernatant was mixed with 60 μL of methanol containing the internal standard and diluted for quantitation analysis using the TQS UPLC–MS/MS system, the electrospray ionization source, and the UPLC BEH HILIC column (Waters) with conditions shown in Supporting Information Table S3. The Cho and ChoP standards (Tan-Mo Technology) and deuterated internal standards (Toronto Research Chemicals) were diluted in methanol to prepare stock solutions. The standard curves were prepared by diluting Cho and ChoP stock solution into different concentrations. Quality control solutions were prepared for both Cho and ChoP. 20 μL of standards was mixed with 60 μL of the corresponding internal standards and was diluted 10-fold before analysis. MassLynx software (version 4.1, Waters) was used for data acquisition and processing.

2.10. In silico molecular docking of LPZ with PHOSPHO1 protein and mining of the Small Molecule Suite database for protein–drug affinity information

The structure of LPZ, ChoP, and 2-AG-LPA was downloaded from the ZINC database (<https://zinc.docking.org/>). The 3D structure of the PHOSPHO1 protein was downloaded from the AlphaFold platform. *In silico* molecular docking was performed by cavity-detection guided blind docking¹¹. Affinity and selectivity data of LPZ with PHOSPHO1 and other reported LPZ targets were extracted from the Small Molecule Suite database (<http://www.smallmoleculesuite.org/>)¹².

2.11. RNA isolation, qPCR analysis and Western blotting

Total RNA samples were extracted using the Trizol total RNA extraction kit (Absin). After quantification of RNA concentration using NanoDrop Microvolume Spectrophotometer (ThermoFisher Scientific), 1 μg of RNA was reverse transcribed with a 1st Strand cDNA Synthesis kit (Yeasen Biotechnology). qPCR was performed by Quant Studio 1 (ThermoFisher Scientific) using the SYBR Green-based kit (Absin) and the results were normalized to the housekeeping gene Gapdh/GAPDH and analyzed using $2^{-\Delta\Delta\text{CT}}$ method. Please see Supporting Information Table S4 for the list of mouse and human qPCR primer sequences. Primary antibodies used for Western blot analysis include Vinculin (Cell Signaling Technology) and UCPI (Proteintech).

2.12. Data analysis

An open-access dataset (GSE27949)¹³ was utilized to extract gene expression profiles of adipose tissues from healthy subjects or severely obese patients. The Illumina BaseSpace application¹⁴ was employed to identify down-regulated genes determined by a given gene's statistical significance and consistency across queried datasets. The Enrichr¹⁵ hub applications WikiPathway and IDG Drug Targets were used to identify pathways and drugs associated with the selected genes. The enriched pathways were ranked based on the adjusted P -value, and the identified drugs were ranked according to the combined score, which was computed by multiplying the \log_{10} (P -value) from the Fisher exact test by the Z -score of the deviation from the expected rank. The top 50 ranked drugs were categorized based on their drug classes and counted within each drug class. LPZ was queried against the Drug Signatures Database within the Enrichr hub to obtain its linked genes, which were subjected to ClinVar analysis within the Enrichr hub to get their associated clinical phenotypes. All data are presented as mean \pm standard error of the mean (SEM). GraphPad Prism (version 9, GraphPad Software) was used for statistical analysis. Student's t -test, two-way ANOVA with Šídák's multiple comparisons test, and one-way ANOVA with Tukey's or Dunnett's *post hoc* analysis were applied to calculate the statistical significance, with $P < 0.05$ considered statistically significant.

3. Results

3.1. Association between lansoprazole and obesity

We utilized the Illumina BaseSpace applications¹⁴ and open-access gene expression data¹³ to identify down-regulated genes from adipose tissues of severely obese patients, which were subsequently analyzed by the Enrichr¹⁵ hub applications to determine their

enriched pathways and associated medications. WikiPathway analysis revealed that the selected genes were enriched in pathways like adipogenesis, thermogenesis, fatty acid biosynthesis and metabolism (Fig. 1A). This observation is consistent with reported adipose tissue dysregulation during obesity development¹⁶ and demonstrates the robustness of the analysis. The identified medications were categorized based on respective drug classes and then ranked according to the counts of medications within each class. The listed drug classes (Fig. 1B) cover a broad spectrum of therapeutic areas, including, but not limited to, cancer (kinase inhibitors), female hormone disorders (estrogens, progestins), digestive disorders (PPIs), immune-related conditions (corticosteroids, nonsteroidal anti-inflammatory drugs, disease-modifying anti-rheumatic drug), skin conditions (retinoids), neurological conditions (selective serotonin reuptake inhibitors), and obesity (lipase inhibitors). Except for the lipase inhibitors, which is a class of approved weight-loss agents, many other drug classes are not conventionally known for their association with weight loss, which presents an opportunity to assess their impact on body weight management.

We then focus on PPIs due to their relatively low toxicity compared with antineoplastics, or hormone therapy medications, which pose a risk of cancer and cardiovascular disease if used chronically. Considering the pharmacokinetic profile¹⁷ of the identified PPIs (omeprazole, dexrabeprazole, lansoprazole, rabeprazole), lansoprazole (LPZ) was selected for further studies. We queried LPZ against the Drug Signatures Database and ClinVar

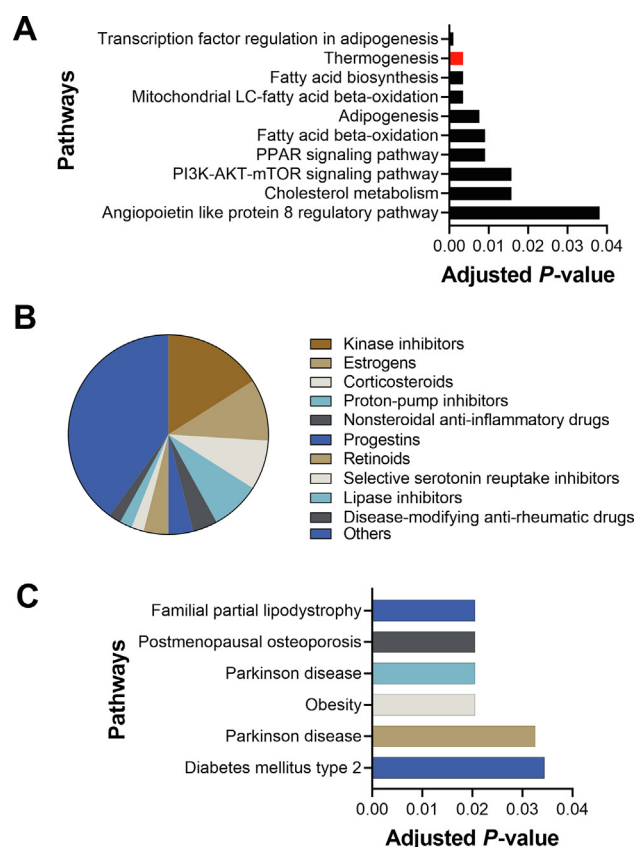


Figure 1 Association between LPZ and obesity. (A) Pathways enriched from down-regulated genes in the adipose tissue of severely obese patients, with thermogenesis representing a top-enriched pathway. (B) Drug classes of medications linked to down-regulated genes in (A). (C) Pathways enriched from LPZ-associated genes.

application within the Enrichr hub to determine its associated genes and clinical phenotypes, which revealed terms related to obesity and diabetes (Fig. 1C). These results prompted us to further investigate the role and underlying mechanisms of LPZ in the development of obesity and related metabolic disorders.

3.2. LPZ protects mice from high-fat diet-induced obesity and type 2 diabetes

We investigated the effect of LPZ on obesity development using a high-fat diet (HFD)-induced obesity model. Male C57BL/6J mice were first fed with HFD for 12 weeks, followed by vehicle or LPZ treatment while remaining on HFD feeding. While the vehicle group continued to gain body weight, LPZ treatment slowed down the body weight increase (Fig. 2A). Since the lean mass was comparable between the vehicle and LPZ treatment group, the reduction of fat mass gain mainly accounted for the body weight difference upon the LPZ treatment (Fig. 2B–D). The body weight homeostasis is regulated by energy intake and expenditure. LPZ treatment did not alter food intake (Fig. 2E), but it significantly induced oxygen consumption and energy expenditure (Fig. 2F), contributing to reduced body weight gain upon HFD feeding. Consistent with increased energy expenditure, LPZ treatment stimulated adipose thermogenesis in obese mice, as reflected by a more thermogenically active adipose morphology and reduced mean adipocyte size (Fig. 2G and H), increased rectal temperature and brown adipose tissue (BAT) temperature (Fig. 2I and J), and higher expression of thermogenic genes in BAT and inguinal adipose tissue (iWAT) (Fig. 2K).

Obesity is a major risk factor for insulin resistance. We further evaluated the effect of LPZ on insulin sensitivity. Consistent with their lean phenotype, the LPZ-treated mice displayed improved glucose tolerance and insulin sensitivity compared with their vehicle-treated counterparts, as assessed by the glucose tolerance test (GTT), insulin tolerance test (ITT) and fasting insulin level (Fig. 2L–N). Additionally, LPZ ameliorated HFD-induced hepatic steatosis, as reflected by reduced fatty degeneration (Fig. 2G). These results indicate that LPZ stimulated adipose thermogenesis and energy expenditure, and protected mice from the progression of pre-existing obesity, insulin resistance and hepatic steatosis upon HFD challenge.

To investigate whether LPZ can prevent obesity development, we switched chow diet-fed male C57BL/6J mice to HFD while simultaneously treated with either vehicle or LPZ. LPZ treatment significantly reduced weight gain (Fig. 3A) and fat mass accumulation (Fig. 3B–D). The effect of LPZ on body weight was likely attributed to increased energy expenditure (Fig. 3F) without affecting the food intake (Fig. 3E). Consistently, LPZ treatment induced thermogenic morphology and expression of thermogenic genes in both BAT and iWAT (Fig. 3G–I), improved glucose tolerance, insulin sensitivity and reduced serum insulin level (Fig. 3J–L). Taken together, we showed that LPZ can both ameliorate pre-existing obesity and prevent mice from developing obesity.

3.3. LPZ stimulates adipose thermogenesis

Since impairment of thermogenesis is closely linked to obesity development, the alleviation of obesity by LPZ prompted us to investigate the effect of LPZ on adipose thermogenesis. To determine the *in vivo* effect of LPZ on adipose thermogenesis, we pre-treated mice with either vehicle or LPZ for one week before

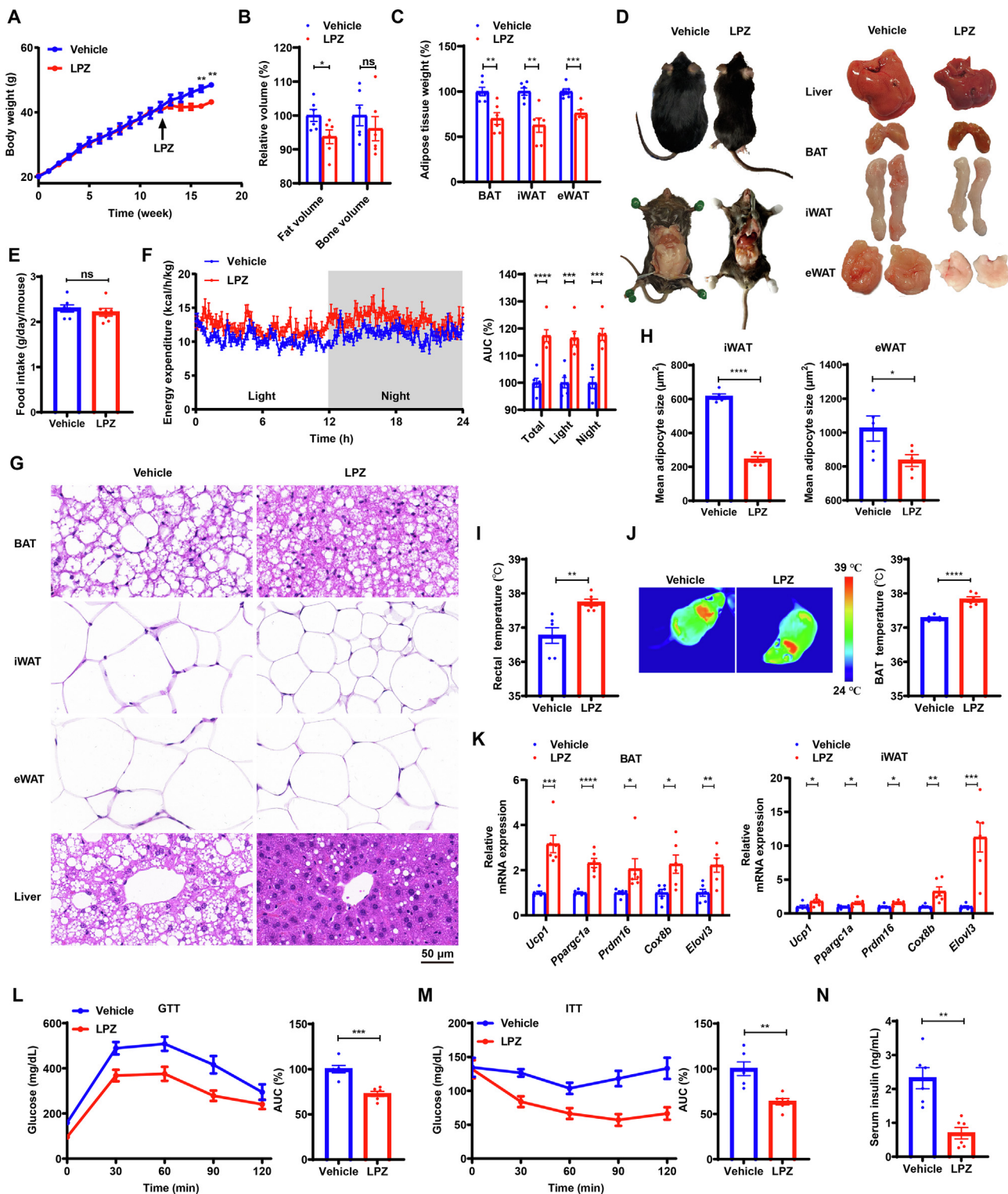


Figure 2 LPZ ameliorated HFD-induced metabolic dysfunctions. (A) Body weight of male C57BL/6J mice fed with HFD for 12 weeks followed by vehicle or 10 mg/kg LPZ treatment ($n = 6$). (B, C) Fat and bone volume and relative weight of different adipose depots of mice in (A). (D) Gross morphology of mice in (A) and macroscopy of adipose tissues and liver. (E) Food intake of HFD-fed mice was recorded every three days following vehicle or LPZ treatment ($n = 7$ measurement time points). (F) Energy expenditure of mice in (A) was measured by indirect calorimetry. (G) Representative H&E staining of adipose depots and liver sections of mice in (A). Scale bar: 50 μ m. (H) Mean adipocyte size of iWAT and eWAT ($n = 5$). (I, J) Rectal temperature, representative infrared thermography images and the brown adipose tissue (BAT) temperature of mice in (A). (K) Thermogenic gene expression in BAT and inguinal white adipose tissue (iWAT) of mice in (A). (L, M) Effect of LPZ on glucose tolerance test (GTT) and insulin tolerance test (ITT) performance of mice on HFD. (N) Effect of LPZ on serum insulin level of mice on HFD. Data are expressed as mean \pm SEM. Student's t -test or two-way ANOVA with Šidák's multiple comparisons test; * $P < 0.05$, ** $P < 0.01$, *** $P < 0.001$, **** $P < 0.0001$; ns, not statistically significant.

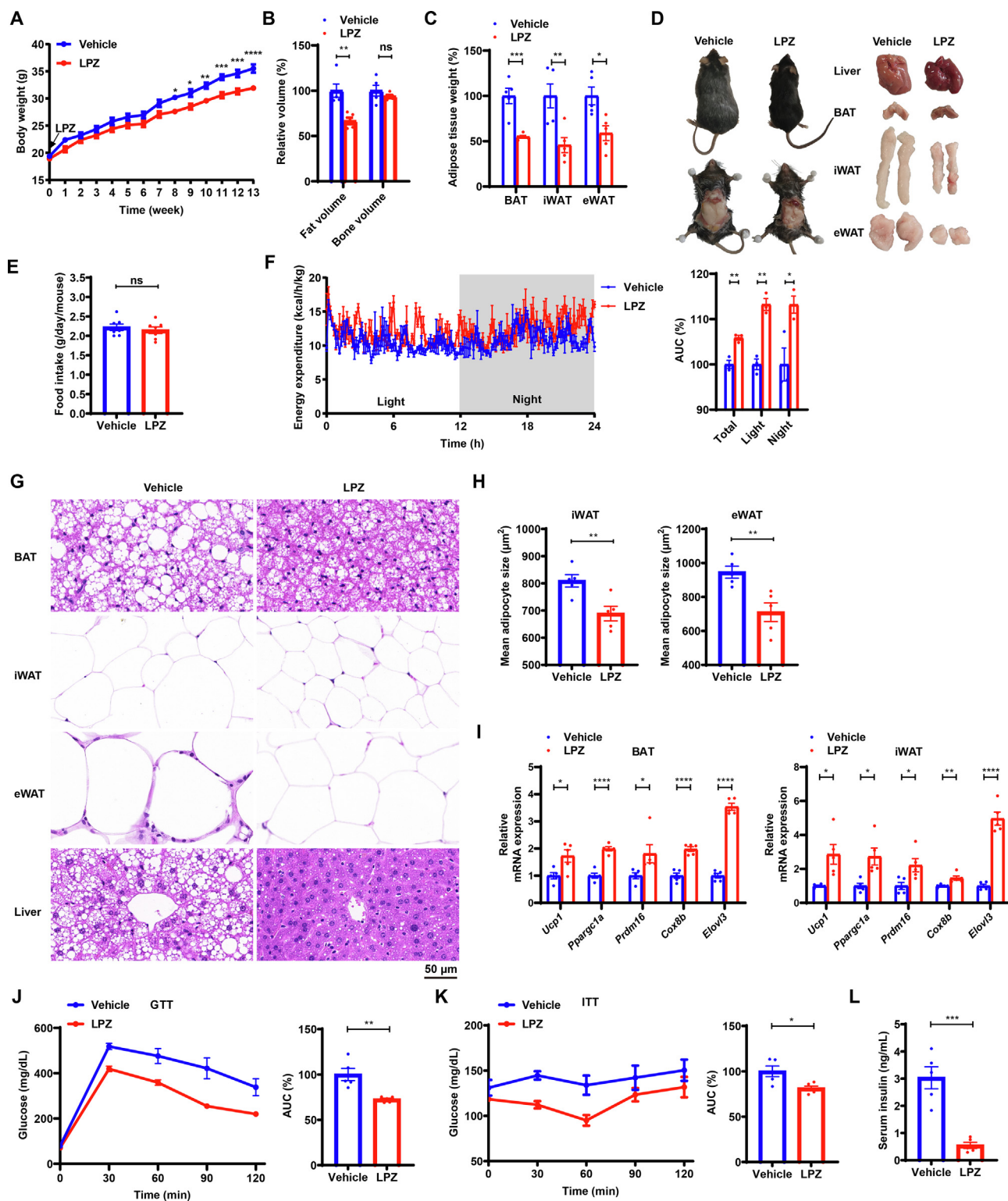


Figure 3 LPZ mitigated the development of obesity and insulin resistance in mice. (A) Body weight of HFD-fed mice simultaneously treated with vehicle or 10 mg/kg LPZ ($n = 5$). (B) Fat and bone volume of mice in (A). (C) Relative weight of different adipose depots following HFD feeding. (D) Gross morphology of mice in (A) and macroscopy of adipose tissues and liver. (E) Food intake of HFD-fed mice was recorded every three days following vehicle or LPZ treatment ($n = 7$ measurement time points). (F) Energy expenditure of mice on HFD ($n = 3$). (G) Representative H&E staining of adipose depots and liver sections of mice on HFD. Scale bar: 50 µm. (H) Mean adipocyte size of iWAT and eWAT of HFD-fed mice. (I) Thermogenic gene expression in iWAT and BAT of mice in (A). (J, K) Effect of LPZ on GTT and ITT performance of mice on HFD. (L) Effect of LPZ on serum insulin level of mice on HFD. Data are expressed as mean \pm SEM. Student's *t*-test or two-way ANOVA with Šidák's multiple comparisons test; * $P < 0.05$, ** $P < 0.01$, *** $P < 0.001$, **** $P < 0.0001$; ns, not statistically significant.

challenging the mice with acute cold exposure at 4 °C. LPZ treatment improved cold tolerance in mice, as indicated by better sustained rectal temperatures during cold exposure (Fig. 4A). Additionally, LPZ treatment significantly increased BAT temperature, as measured by infrared thermography imaging of the surface body temperature of mice around the interscapular area during cold exposure (Fig. 4B and C). In contrast, the tail skin temperature, which was not controlled by adipose thermogenesis, was not affected by LPZ treatment (Fig. 4D). These findings demonstrate that LPZ increased core and BAT temperature in cold-challenged mice without altering heat dissipation from the tail.

Consistent with the cold-tolerant phenotype, LPZ treatment increased the expression of key adipose thermogenic genes, such as *Ucp1*, *Prdm16*, *Ppargc1a*, and *Cox8b*, in both BAT and iWAT following cold exposure (Fig. 4E and F). This effect was further supported by increased UCP1 protein expression in the BAT of

cold-exposed mice (Fig. 4G). Histological analysis by H&E staining revealed that BAT and iWAT from LPZ-treated mice contained smaller adipocytes with multilocular lipid droplets, indicating thermogenically active BAT and beigeing in iWAT (Fig. 4H). These results suggest that LPZ promotes adipose thermogenesis and cold tolerance.

To investigate the LPZ-induced thermogenic effect at the cellular level, we treated primary mouse adipocytes with either vehicle or LPZ and evaluated their mitochondrial respiratory activities. LPZ treatment caused a significant increase in basal, maximal and proton leak respiration in both BAT- and iWAT-derived primary adipocytes compared with their vehicle-treated counterparts (Fig. 5A, B, D and E). Consistently, LPZ treatment elevated the expression of thermogenic genes in both BAT- and iWAT-derived primary adipocytes (Fig. 5C and F), supporting the cell-autonomous effect of LPZ. To explore the human relevance of

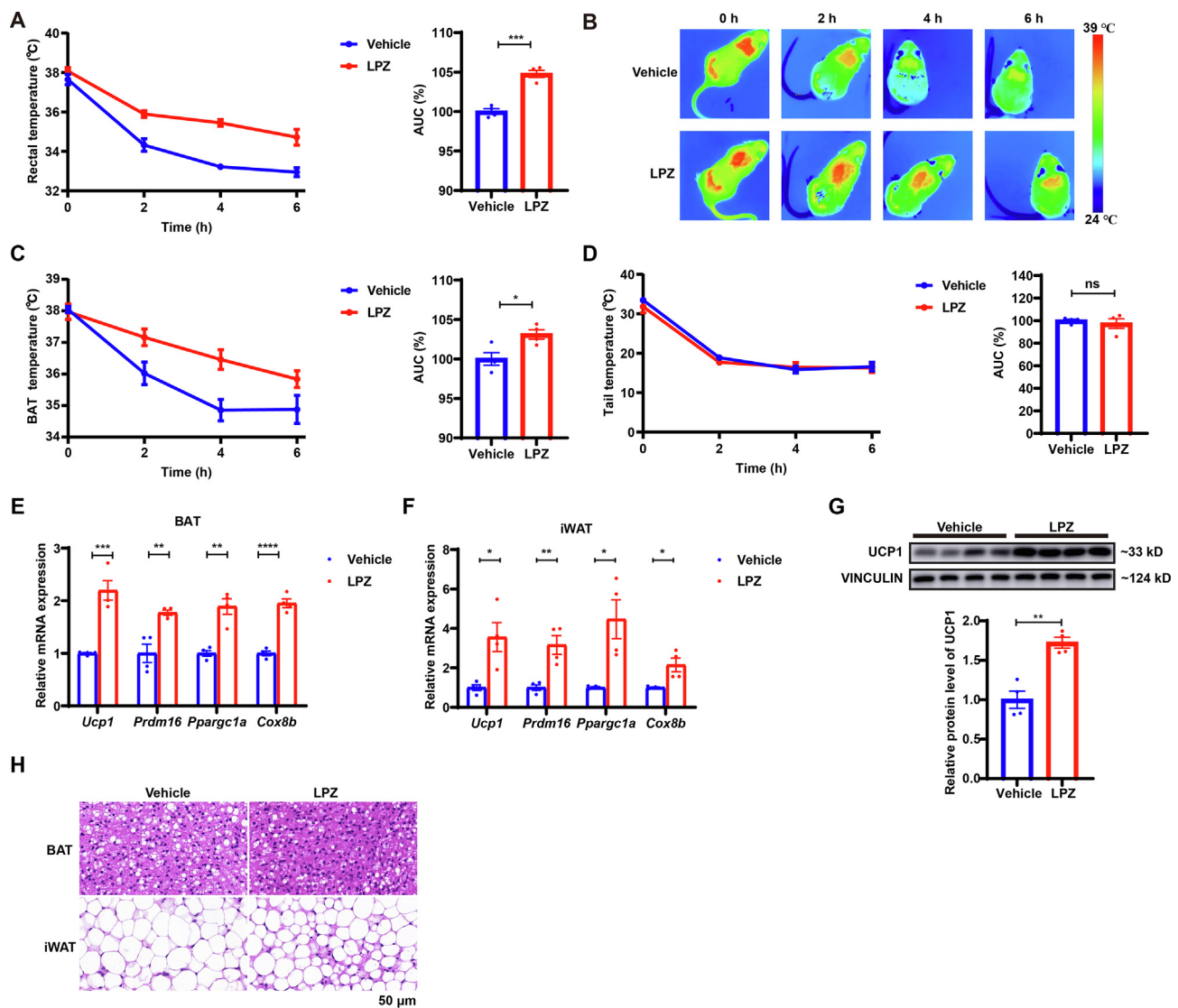


Figure 4 LPZ induced cold tolerance and adipose thermogenesis in mice. (A) The rectal temperature and corresponding AUC of vehicle- and LPZ (10 mg/kg)-treated mice during acute cold exposure ($n = 4$). (B)–(D) Representative infrared thermography images, BAT temperature and tail temperature of mice in (A). (E, F) mRNA expression of adipose thermogenesis-related genes in BAT and iWAT of cold-exposed mice. (G) Protein expression of UCP1 in BAT of mice in (A). (H) Representative H&E staining of BAT and iWAT sections of cold-exposed mice. Scale bar: 50 μm . Data are expressed as mean \pm SEM. Student's t -test; * $P < 0.05$, ** $P < 0.01$, *** $P < 0.001$, **** $P < 0.0001$; ns, not statistically significant.

LPZ-stimulated adipose thermogenesis, we treated primary adipocytes from human white adipose tissue with either vehicle or LPZ and found that LPZ can also induce the expression of thermogenic markers *UCP1* and *PPARGC1A* in these cells (Fig. 5G).

3.4. LPZ efficiently inhibits *PHOSPHO1* activity in mouse adipose tissues and primary adipocytes

PHOSPHO1 was identified as a molecular target inhibited by LPZ with relatively high affinity among other reported LPZ

targets^{12,18,19} (Fig. 6A). We employed the AlphaFold platform²⁰ to obtain the 3D structure of mouse *PHOSPHO1* protein based on its amino acid sequence. Molecular docking analysis revealed that LPZ binds to the AlphaFold-predicted *PHOSPHO1* protein with lower binding energy than phosphocholine, the natural substrate of *PHOSPHO1* (Fig. 6B–D).

The docking analysis of the *PHOSPHO1* protein and (*R*)-LPZ revealed specific interactions between the two molecules. The trifluoromethoxy oxygen group of (*R*)-LPZ made hydrophobic contact with the residues PRO227 and TYR226 of *PHOSPHO1*,

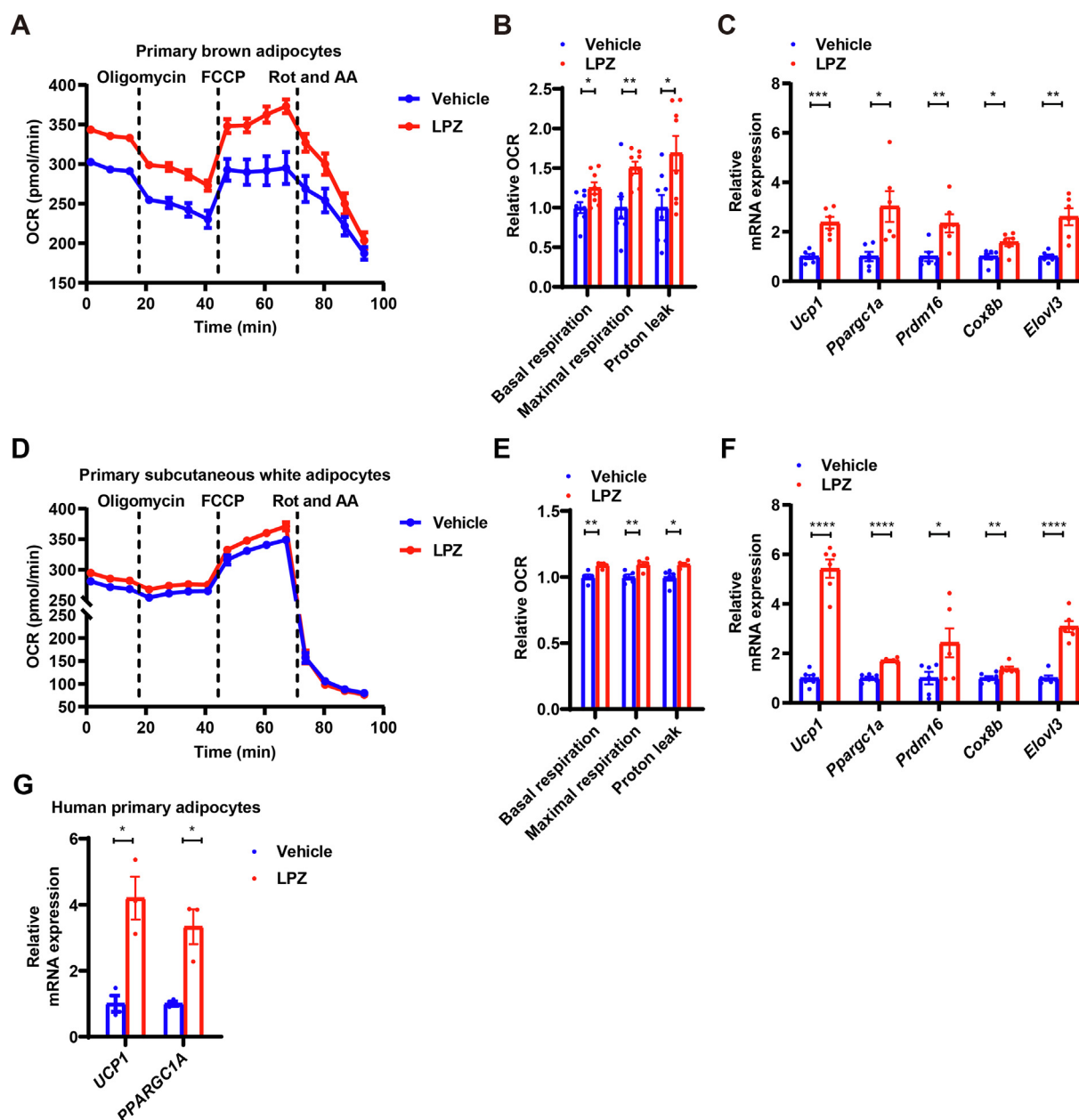


Figure 5 LPZ stimulated thermogenesis in mouse and human primary adipocytes. (A, B) Oxygen consumption rate and relative respiration fraction of mouse primary brown adipocytes treated with vehicle or LPZ ($n = 8$). (C) Effect of LPZ on thermogenic gene expression in mouse primary brown adipocytes ($n = 6$). (D, E) Oxygen consumption rate and relative respiration fraction of mouse primary subcutaneous white adipocytes treated with vehicle or LPZ ($n = 5$). (F) Effect of LPZ on thermogenic gene expression in mouse primary subcutaneous white adipocytes ($n = 6$). (G) Thermogenic gene expression in human primary adipocytes treated with vehicle or LPZ ($n = 3$). 10 $\mu\text{mol/L}$ LPZ was administered throughout the experiments. Rot, rotenone; Ant, antimycin A. Data are expressed as mean \pm SEM. Student's *t*-test; * $P < 0.05$, ** $P < 0.01$, *** $P < 0.001$, **** $P < 0.0001$.

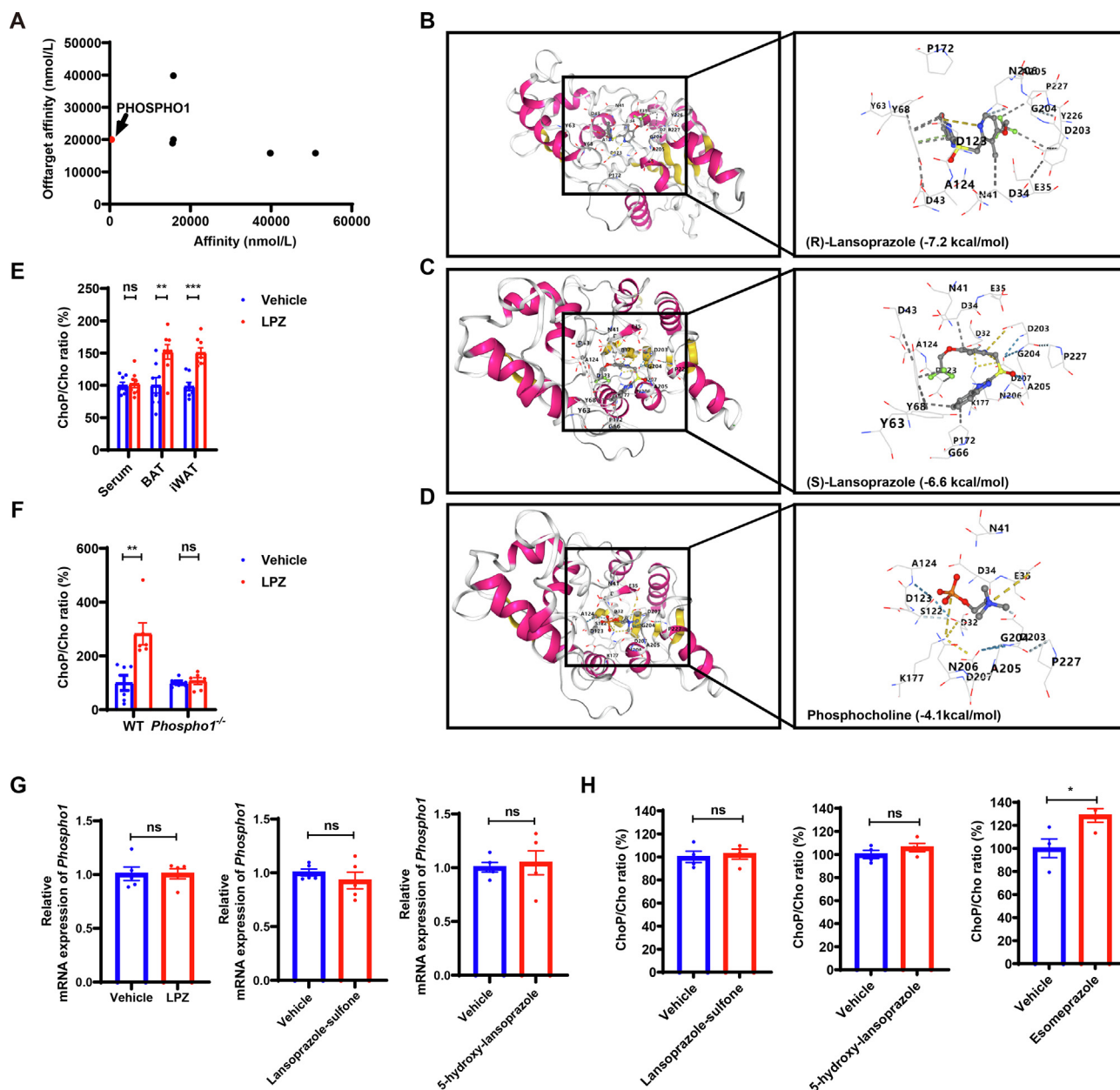


Figure 6 Inhibitory effect of LPZ on PHOSPHO1. (A) Affinity and selectivity of LPZ with PHOSPHO1 and other reported LPZ targets from the small molecule suite database. (B)–(D) Molecular docking of mouse PHOSPHO1 protein with (R)-LPZ, (S)-LPZ, and phosphocholine. The 3D structure of mouse PHOSPHO1 protein was predicted by AlphaFold. Pink and yellow colors represent α -helices and β -sheets, respectively. (E) The ratio of phosphocholine/choline (ChoP/Cho) was measured by UPLC–MS/MS in mouse serum, BAT, and iWAT ($n = 8$). The vehicle groups were normalized to 100%. (F) Effect of LPZ (10 μ M) on the relative ratio of ChoP/Cho in inguinal primary adipocytes from wild-type (WT) mice and *Phospho1*^{-/-} mice ($n = 6$). The vehicle groups were normalized to 100%. (G) Effect of LPZ, lansoprazole-sulfone and 5-hydroxy-lansoprazole on mRNA expression of *Phospho1* ($n = 5$). (H) Effect of lansoprazole-sulfone, 5-hydroxy-lansoprazole and esomeprazole on the relative ratio of ChoP/Cho in primary adipocytes ($n = 4$). The vehicle groups were normalized to 100%. Data are expressed as mean \pm SEM. Student's *t*-test; * $P < 0.05$, ** $P < 0.01$, *** $P < 0.001$; ns, not statistically significant.

while the methyl group also formed a hydrophobic interaction with the residue ASP34. The hydrophobic benzimidazole moiety of (R)-LPZ interacted with the residue TYR68 through hydrophobic contact and pi–pi stacking. The pyridine ring of (R)-LPZ formed a weak hydrogen bond with the residue ASN206 and an ionic interaction with the residue ASP123.

To measure the enzymatic activity of PHOSPHO1, we developed the UPLC–MS/MS method to simultaneously quantify

phosphocholine (ChoP) and choline (Cho) in biological samples based on the internal standard method. Under optimized chromatography conditions (Table S3), we were able to detect both ChoP and Cho in the mouse serum, adipose tissues and primary adipocytes. The chromatographic peaks and retention times of Cho, deuterated Cho (Cho-d9), ChoP and deuterated ChoP (ChoP-d9) are shown in Supporting Information Fig. S1. The intra-day and inter-day accuracy and precision of Cho and

ChoP are shown in [Supporting Information Table S5](#). The linearity of the UPLC–MS/MS method is shown in [Supporting Information Fig. S2](#). The activity of PHOSPHO1 was assessed by calculating the ratio of ChoP/Cho, given that PHOSPHO1 hydrolyzes ChoP to produce Cho and phosphate. The ratio of ChoP/Cho was found elevated in the iWAT and BAT of LPZ-treated mice, as well as in LPZ-treated primary mouse adipocytes, but not in the serum of LPZ-treated mice ([Fig. 6E and F](#)). The inhibitory effect of LPZ was PHOSPHO1-dependent, because the induction of ChoP/Cho ratio was abolished in adipocytes isolated from *Phospho1*^{−/−} mice ([Fig. 6F](#)). In addition, we assessed the mRNA expression of *Phospho1* in primary adipocytes and revealed that LPZ, as well as its metabolites, 5-hydroxy-lansoprazole and lansoprazole-sulfone, had no impact on the transcript expression of *Phospho1* ([Fig. 6G](#)). Furthermore, these LPZ metabolites also did not affect the enzymatic activity of PHOSPHO1, as indicated by the ChoP/Cho ratio ([Fig. 6H](#)). Accordingly, LPZ may inhibit PHOSPHO1 activity without altering its expression, which halts when LPZ is metabolized into 5-hydroxy-lansoprazole or lansoprazole-sulfone. Given the structural similarities shared by all PPIs, including LPZ, we analyzed the effect of esomeprazole, another PPI, on PHOSPHO1 activity. Like LPZ, esomeprazole also elevated the ratio of ChoP/Cho ([Fig. 6H](#)), suggesting that the inhibitory effect on PHOSPHO1 activity and the potential anti-obesity benefits may not be limited to LPZ. Further structural and functional studies are necessary to elucidate the structural requirements for inhibiting PHOSPHO1 activity.

3.5. The LPZ-induced metabolic benefits are PHOSPHO1-dependent

To determine whether PHOSPHO1 is required for the observed metabolic benefits induced by LPZ, we employed *Phospho1*^{−/−} mice as a loss-of-function model to evaluate LPZ-mediated metabolic effects. Ablation of *Phospho1* completely abolished the LPZ-induced cold tolerance and expression of thermogenic genes both *in vivo* ([Fig. 7A–D](#)) and in primary adipocytes ([Fig. 7E–G](#)). The LPZ-mediated protection against HFD-induced obesity, insulin resistance, and hepatic steatosis was also abolished in *Phospho1*^{−/−} mice ([Fig. 8](#)). *Phospho1*^{−/−} mice were previously observed to exhibit cold tolerance and were resistant to obesity development⁹. Our findings indicate that LPZ treatment no longer exerts additional enhancements in cold tolerance or obesity resistance in *Phospho1*^{−/−} mice, suggesting that PHOSPHO1 primarily mediates the metabolic benefits of LPZ.

3.6. The metabolic basis of LPZ-induced adipose thermogenesis

Metabolomic analysis provides a comprehensive understanding of drug-induced metabolic changes in biological systems, making it a crucial tool for unraveling mechanisms of action²¹. PHOSPHO1 belongs to the haloacid dehalogenase superfamily, which hydrolyzes the C–OP bond of multiple substrates²². We analyzed changes in paired phosphorylated/unphosphorylated metabolites upon LPZ treatment to identify potential downstream metabolic mediators of LPZ-regulated thermogenesis by metabolomics profiling. Interestingly, we observed an increased ratio of 2-AG-LPA/2-AG in adipose tissues of mice either upon the LPZ treatment or with *Phospho1* ablation ([Fig. 9A–C](#)). 2-AG is a known endogenous agonist of the cannabinoid receptor type 1 (CB1), which has been reported to negatively regulate adipose thermogenesis^{23,24}. Molecular docking simulation predicted that

the binding energy between 2-AG-LPA and PHOSPHO1 is −6.1 kcal/mol, which is lower than that with phosphocholine, the well-known endogenous substrate of PHOSPHO1 ([Fig. 9D](#)). The docking simulation of the PHOSPHO1 protein with 2-AG-LPA revealed the presence of hydrogen bonds formed between the oxygen atom on the phosphate group of 2-AG-LPA and amino acid residues ASP203 and GLU35 of PHOSPHO1. In addition, the oxygen atom on the hydroxyl group of 2-AG-LPA formed hydrogen bonds with amino acid residues ASP34 and SER122 of PHOSPHO1. The fatty acyl chain of 2-AG-LPA exhibited hydrophobic interactions with amino acid residues TYR68, PRO172 and ASN206 of PHOSPHO1 ([Fig. 9D](#)). To determine whether a reduction in 2-AG levels contributes to the increased thermogenesis following LPZ treatment, we treated primary adipocytes with 2-AG and observed a reduction of *Ucp1* expression and cellular respiration ([Fig. 9E and F](#)). In order to investigate the role of the CB1 in mediating the effects of 2-AG, we utilized a pharmacological antagonist of CB1-Rimonabant to block the receptor activity, which effectively reversed the effect of 2-AG on *Ucp1* expression in primary adipocytes ([Fig. 9E](#)). The inhibitory effect of 2-AG on *Ucp1* expression remained unaffected in the presence of LPZ or the ablation of *Phospho1* ([Fig. 9G and H](#)). In addition, this effect appeared to be 2-AG specific, as treatment with an equal concentration of choline, which is the natural enzymatic product resulting from the hydrolysis of phosphocholine by PHOSPHO1, did not alter the mRNA expression of *Ucp1* or cellular respiration in primary adipocytes ([Fig. 9F and I](#)). Our results suggested that LPZ may have suppressed CB1 activity by restricting the availability of 2-AG, thereby promoting adipose thermogenesis ([Fig. 9J](#)).

4. Discussion

Drug repurposing offers an effective approach for new therapeutic application discovery, considering the reduced drug development timeline, cost, and well-documented safety profiles. In this study, we identified that LPZ, a commonly prescribed drug for gastrointestinal ulcers, is associated with obesity by bioinformatic analysis. Therefore, we repurposed LPZ to stimulate the energy-intensive adipose thermogenesis and energy expenditure in primary adipocytes, cold-exposed mice, and high-fat diet-fed mice. Our study reveals for the first time that LPZ treatment enhanced the expression of thermogenic genes, and improved cold tolerance and energy expenditure, which protected mice against HFD-induced obesity, insulin resistance and fatty liver development, emphasizing the importance of fostering drug repurposing endeavors.

LPZ has been reported to reduce body weight gain, improve glucose tolerance in HFD-fed mice^{25,26}, ameliorate hepatic steatosis in the hypercholesterolemic rat model²⁷, lower circulating glucose in the diabetic gerbil *Psammomys obesus*²⁸, and synergized with antidiabetic medications to improve glycemic control^{25,29}. Clinical studies have also reported that lansoprazole treatment improved glycemic control in diabetic patients^{30,31}. However, the molecular mechanism for the metabolic benefits of LPZ remains largely unknown. We have previously established PHOSPHO1, a phosphoethanolamine and phosphocholine phosphatase, as an important negative regulator of adipose thermogenesis. Loss of function of *Phospho1* resulted in increased expression of adipose thermogenic genes, improved cold tolerance and energy expenditure, and alleviated obesity and insulin resistance induced by HFD feeding in mice⁹. These results suggested

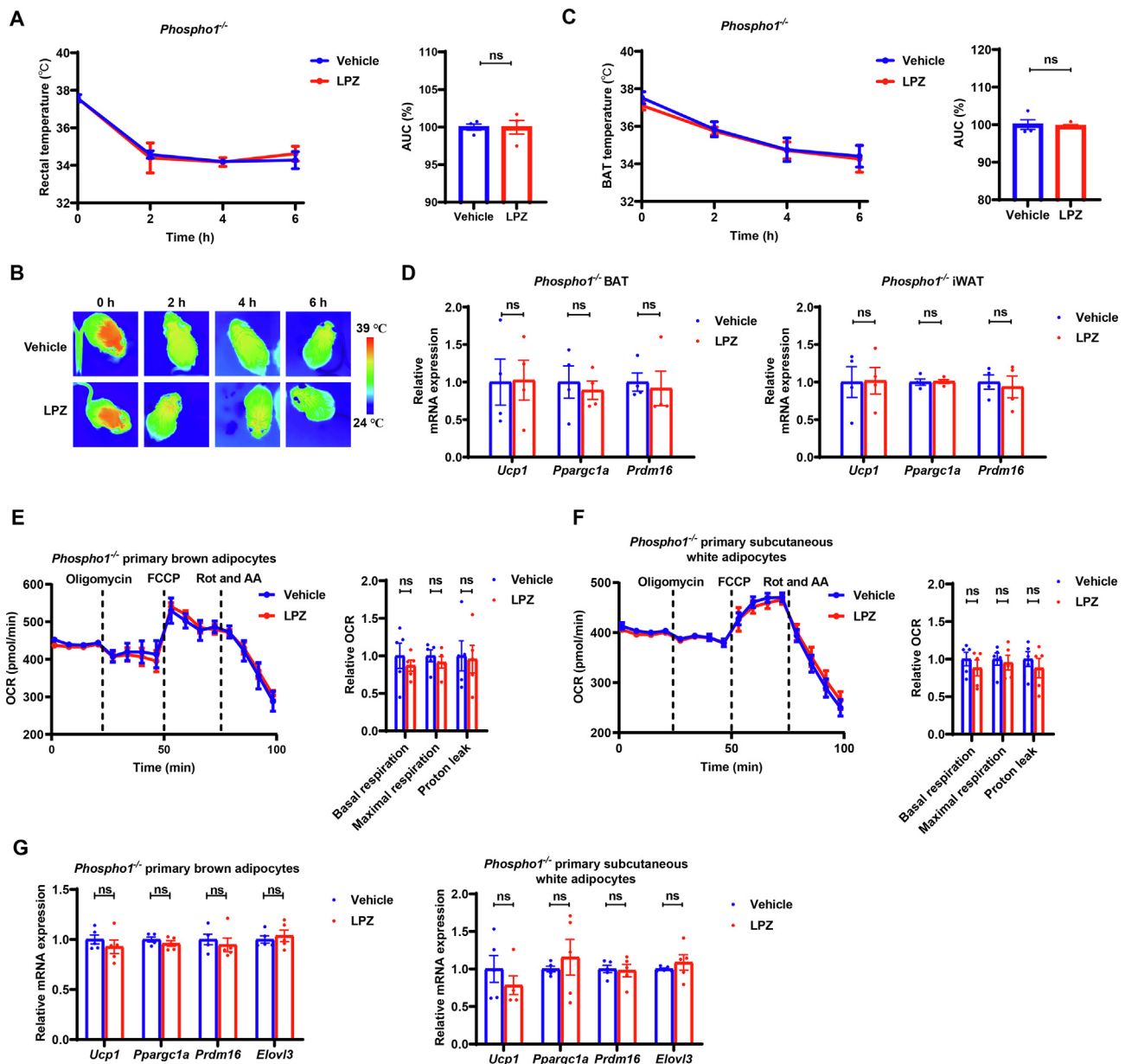


Figure 7 The LPZ-induced adipose thermogenesis was dependent on PHOSPHO1. (A)–(C) The rectal temperature, representative infrared thermography images and BAT temperature of vehicle- and LPZ (10 mg/kg)-treated *Phospho1*^{-/-} mice during cold exposure ($n = 4$). (D) Thermogenic gene expression in vehicle- and LPZ-treated *Phospho1*^{-/-} mice in (A). (E)–(G) Oxygen consumption rate, relative respiration fraction and thermogenic gene expression of BAT- and iWAT-derived *Phospho1*^{-/-} primary adipocytes treated with vehicle or LPZ ($n = 5$). Data are expressed as mean \pm SEM. Student's *t*-test; ns, not statistically significant.

that pharmacological inhibition of PHOSPHO1 could provide a therapeutic approach for obesity and related comorbidities^{32,33}. In the current study, we demonstrate that LPZ stimulates adipose thermogenesis by inhibiting PHOSPHO1. Molecular docking predicted efficient binding between LPZ and PHOSPHO1 protein. Treatment of LPZ inhibited the enzymatic conversion of PHOSPHO1 substrates without changing *Phospho1* expression. LPZ treatment ignited adipose thermogenesis both *in vivo* and in primary adipocytes, as evidenced by the activated core body and BAT temperature, adipose tissue histology and thermogenic gene expression, which were accompanied by increased energy expenditure and improved insulin sensitivity, phenocopying the

metabolic benefits observed in *Phospho1* null mice. Mouse primary adipocytes treated with LPZ exhibited similar changes in the mRNA expression of thermogenic genes and oxygen consumption, indicating a cell-autonomous regulation triggered by LPZ. A similar pattern of effect was observed in LPZ-treated primary human adipocytes. Most importantly, we showed that the metabolic benefits of LPZ were PHOSPHO1-dependent, clearly establishing PHOSPHO1 as the therapeutic target of LPZ.

Our study focused on the role of LPZ-mediated inhibition of PHOSPHO1 in regulating adipose thermogenesis, given the relatively high expression of PHOSPHO1 in thermogenic adipose tissue in mice⁹. Nevertheless, the metabolic benefits of LPZ may

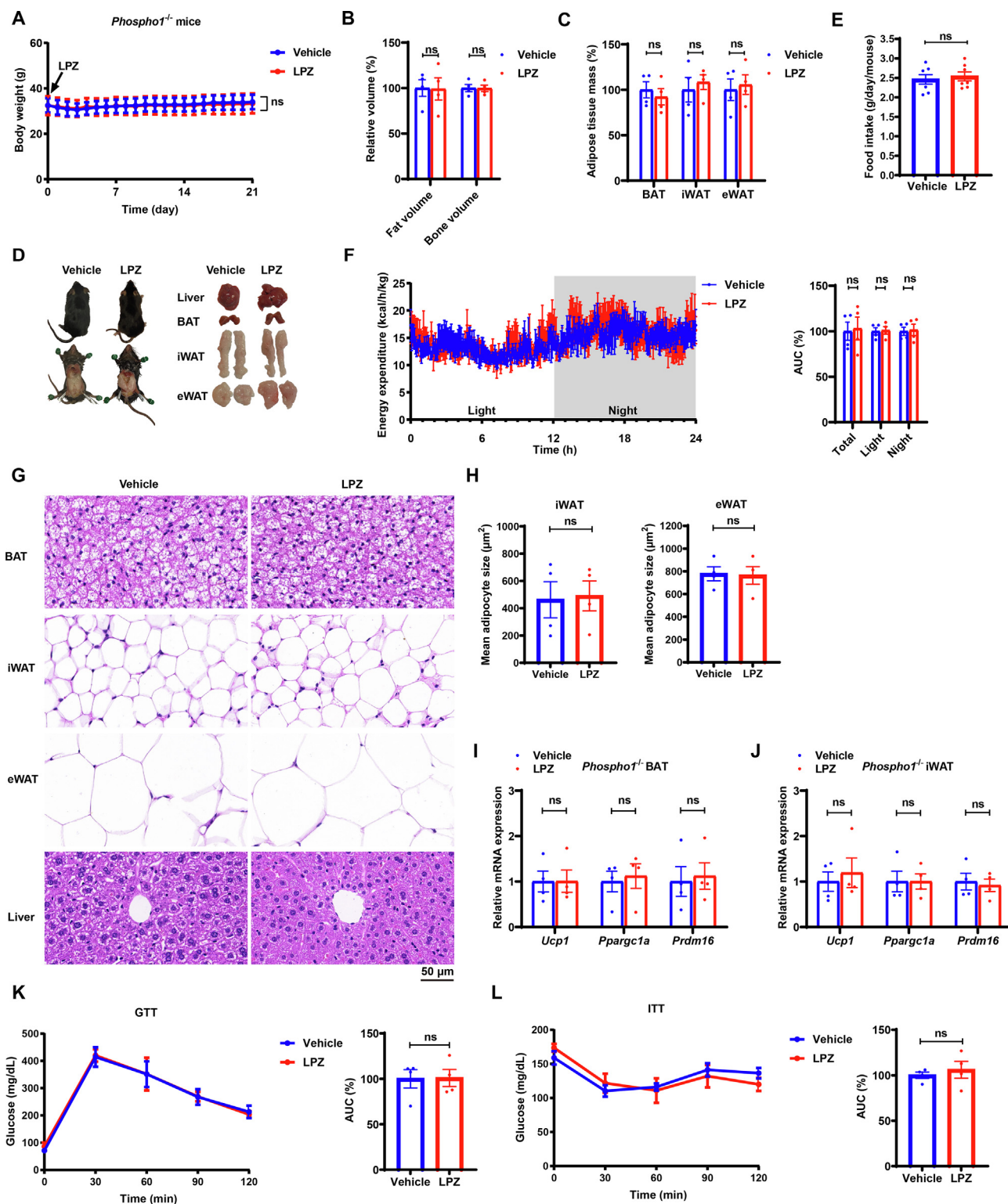


Figure 8 The LPZ-induced metabolic benefit was dependent on PHOSPHO1. (A) Body weight of male *Phospho1^{-/-}* mice fed with HFD followed by vehicle or LPZ (10 mg/kg) treatment ($n = 4$). (B, C) Fat and bone volume and relative weight of different adipose depots of mice in (A). (D) Gross morphology of mice in (A) and macroscopy of adipose tissues and liver. (E) Food intake of HFD-fed mice was recorded every three days following vehicle or LPZ treatment ($n = 7$ measurement time points). (F) Energy expenditure of mice in (A) was measured by indirect calorimetry. (G) Representative H&E staining of adipose depots and liver sections of mice in (A). Scale bar: 50 μ m. (H) Mean adipocyte size of iWAT and eWAT of mice in (A). (I, J) Thermogenic gene expression in iWAT and BAT of mice in (A). (K, L) GTT and ITT of mice in (A). Data are expressed as mean \pm SEM. Student's *t*-test or two-way ANOVA with Šidák's multiple comparisons test; ns, not statistically significant.

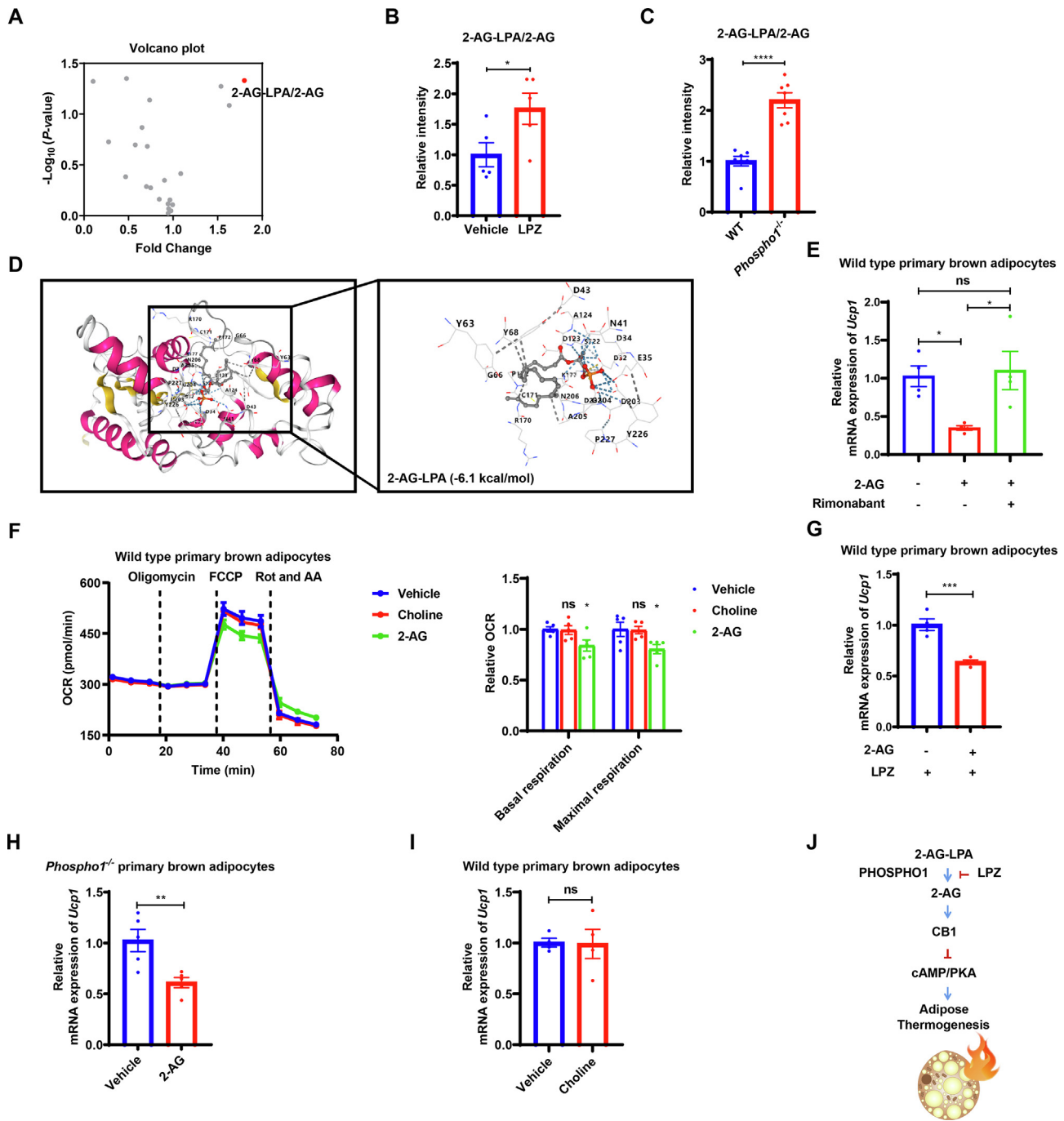


Figure 9 The metabolic basis of LPZ-induced adipose thermogenesis. (A) Average relative abundance of paired phosphorylated/unphosphorylated metabolites in BAT of mice upon LPZ (10 mg/kg) treatment. (B) LPZ induced the relative abundance of 2-AG-LPA/2-AG in BAT of mice ($n = 5$). (C) Relative abundance of 2-AG-LPA/2-AG in BAT of *Phospho1*^{-/-} mice and their wild-type counterparts ($n = 7$). (D) Molecular docking of mouse PHOSPHO1 protein with 2-AG-LPA. (E) Effect of 2-AG (0.1 $\mu\text{mol/L}$) and rimonabant (20 $\mu\text{mol/L}$) on *Ucp1* expression in mouse primary brown adipocytes ($n = 4$). (F) Oxygen consumption rate and relative respiration fraction of BAT-derived primary adipocytes treated with vehicle, 0.1 $\mu\text{mol/L}$ 2-AG, or 0.1 $\mu\text{mol/L}$ choline ($n = 5$). (G) 2-AG (0.1 $\mu\text{mol/L}$) reduced *Ucp1* expression in the presence of LPZ (10 $\mu\text{mol/L}$) ($n = 4$). (H) Effect of 2-AG (0.1 $\mu\text{mol/L}$) on the relative mRNA expression of *Ucp1* in *Phospho1*^{-/-} primary brown adipocytes ($n = 5$). (I) Effect of choline (0.1 $\mu\text{mol/L}$) on the relative mRNA expression of *Ucp1* in wild-type primary brown adipocytes ($n = 4$). (J) Schematic diagram illustrating the potential mechanisms of LPZ-induced adipose thermogenesis. Data are expressed as mean \pm SEM. Student's *t*-test or one-way ANOVA with Tukey's or Dunnett's *post hoc* analysis, * $P < 0.05$, ** $P < 0.01$, *** $P < 0.001$, **** $P < 0.0001$; ns, not statistically significant.

extend to other metabolic tissues, such as the liver and muscle. Indeed, we have observed that LPZ treatment ameliorated HFD-induced liver steatosis and improved GTT and ITT performance in mice. Whether these effects are directly induced by LPZ treatment or are secondary to LPZ-improved adipose thermogenesis warrants further investigation. Future studies employing tissue-specific PHOSPHO1 knockout mice could provide valuable insights into the specific metabolic tissues that contribute to the metabolic actions of LPZ *in vivo* and refine our understanding of the broader metabolic implications of LPZ beyond its impact on adipose thermogenesis.

Interestingly, the reported anti-obesity effect induced by LPZ was achieved at a high dose (200 mg/kg) by gastric gavage in mice, which was not attributed to changes in visceral adipose tissue mass²⁶. In our study, subcutaneous injection of 10 mg/kg LPZ efficiently reduced body weight and visceral fat mass gain in mice challenged with HFD. These discrepancies may be due to different drug administration routes. When administered by gastric gavage, LPZ is activated by the acidic environment of the stomach, where the protonated active metabolite of LPZ covalently binds to and inhibits gastric H⁺-K⁺-ATPase from working as a PPI. On the other hand, the subcutaneous delivery of LPZ circumvents its gastric activation and enteral absorption. LPZ is absorbed locally and likely in its parent form, sustaining its effect of PHOSPHO1 inhibition and activating adipose thermogenesis. In addition, the expression of the original target of LPZ, the gastric H⁺-K⁺-ATPase, is mainly restricted in the stomach³⁴, whereas the mouse and human *PHOSPHO1* transcripts were highly enriched in BAT and induced by thermogenic stimuli such as cold exposure and isoproterenol treatment⁹. Therefore, the LPZ-activated adipose thermogenesis is likely mainly mediated by PHOSPHO1. However, we could not exclude the possibility that molecular targets other than PHOSPHO1 may have also contributed to the metabolic benefits of LPZ.

One of the advantages of drug repurposing is the available comprehensive drug safety information. Long-term treatment with LPZ has been reported to be well tolerated in patients³⁵. Depletion of PHOSPHO1 was not associated with developmental abnormalities in adult mice³². Nevertheless, further functional and toxicological evaluations need to be carried out with LPZ and other PHOSPHO1 inhibitors to assess their safety and effectiveness in treating metabolic disorders.

Another key novelty of the current study is the metabolic basis underlying the metabolic benefits of LPZ. Although choline is the well-known endogenous enzymatic product of PHOSPHO1 resulting from the hydrolysis of phosphocholine, we were surprised to find that treatment with choline had little effect on the mRNA expression of *Ucp1* or cellular respiration in primary adipocytes. Instead, our metabolomics analysis of paired phosphorylated/unphosphorylated metabolites revealed that LPZ increased the ratio of 2-AG-LPA/2-AG in adipose tissue. The increased ratio of 2-AG-LPA/2-AG was also observed in *Phospho1*^{-/-} mice, suggesting the effect of LPZ on the 2-AG-LPA/2-AG ratio was mediated by its inhibition of *Phospho1*. Our results suggest that PHOSPHO1 may be involved in converting 2-AG-LPA to 2-AG, but future experiments are necessary to characterize 2-AG-LPA as a novel substrate of PHOSPHO1. Nevertheless, the decreased level of 2-AG in LPZ-treated mice was mechanistically important. 2-AG is known to activate CB1, which can negatively regulate cAMP/PKA signaling and thermogenesis in adipose tissue^{23,24}. In agreement with this reasoning, we observed enhanced *Ucp1* expression and thermogenic activities in adipocytes in response to LPZ treatment,

which was attenuated by co-treatment of 2-AG. The selective CB1 antagonist Rimonabant completely abolished the effect of 2-AG on *Ucp1* expression, indicating that the observed effect of 2-AG was mediated through its activation of the CB1 receptor.

5. Conclusions

We identified the novel function and defined the mechanism of LPZ in stimulating adipose thermogenesis and inhibiting diet-induced obesity and insulin resistance. Since LPZ is an FDA-approved, low-cost generic drug, repurposing LPZ may save a significant amount of time and cost in developing novel pharmaceuticals to combat obesity and its associated metabolic disorders.

Acknowledgment

We would like to thank Professor Colin Farquharson of the University of Edinburgh for generously providing us with the *Phospho1*^{-/-} mice. Additionally, we extend our thanks to Dr. Bangxiang Xie from Beijing YouAn Hospital and Jingjing Wang from the animal facility at Capital Medical University for their invaluable technical support and assistance. This work was supported by the Beijing Municipal Natural Science Foundation Grant 7212148 (to Mengxi Jiang, China), the National Natural Science Foundation of China Grant 82000807 (to Mengxi Jiang, China), and the Beijing Municipal Education Commission Grant KM202110025023 (to Mengxi Jiang, China).

Author contributions

Mengxi Jiang initiated and guided this research. Mengxi Jiang and Wen Xie designed the study and wrote the manuscript. Yingting Wu, Jiaqi Xin, Xinyu Li, Ting Yang, Yi Liu, and Yongsheng Zhao performed experiments, analyzed data and generated figures and tables. The final manuscript was reviewed and approved by all authors.

Conflicts of interest

The authors declare no conflicts of interest.

Appendix A. Supporting information

Supporting data to this article can be found online at <https://doi.org/10.1016/j.apsb.2024.01.001>.

References

1. Ansari S, Haboubi H, Haboubi N. Adult obesity complications: challenges and clinical impact. *Ther Adv Endocrinol Metab* 2020;**11**: 2042018820934955.
2. Thereaux J, Lesuffleur T, Czernichow S, Basdevant A, Msika S, Nocca D, et al. Long-term adverse events after sleeve gastrectomy or gastric bypass: a 7-year nationwide, observational, population-based, cohort study. *Lancet Diabetes Endocrinol* 2019;**7**:786–95.
3. Tak YJ, Lee SY. Long-term efficacy and safety of anti-obesity treatment: where do we stand?. *Curr Obes Rep* 2021;**10**:14–30.
4. Cohen P, Kajimura S. The cellular and functional complexity of thermogenic fat. *Nat Rev Mol Cell Biol* 2021;**22**:393–409.
5. Pan R, Zhu X, Maretich P, Chen Y. Combating obesity with thermogenic fat: current challenges and advancements. *Front Endocrinol (Lausanne)* 2020;**11**:185.

6. Yadav MC, Simão AM, Narisawa S, Huesa C, McKee MD, Farquharson C, et al. Loss of skeletal mineralization by the simultaneous ablation of PHOSPHO1 and alkaline phosphatase function: a unified model of the mechanisms of initiation of skeletal calcification. *J Bone Miner Res* 2011;**26**:286–97.
7. Gremse DA. Lansoprazole: pharmacokinetics, pharmacodynamics and clinical uses. *Expert Opin Pharmacother* 2001;**2**:1663–70.
8. Reagan-Shaw S, Nihal M, Ahmad N. Dose translation from animal to human studies revisited. *FASEB J* 2008;**22**:659–61.
9. Jiang M, Chavarria TE, Yuan B, Lodish HF, Huang NJ. Phosphocholine accumulation and PHOSPHO1 depletion promote adipose tissue thermogenesis. *Proc Natl Acad Sci U S A* 2020;**117**:15055–65.
10. Lee MJ, Fried SK. Optimal protocol for the differentiation and metabolic analysis of human adipose stromal cells. *Methods Enzymol* 2014;**538**:49–65.
11. Liu Y, Yang X, Gan J, Chen S, Xiao ZX, Cao Y. CB-Dock2: improved protein–ligand blind docking by integrating cavity detection, docking and homologous template fitting. *Nucleic Acids Res* 2022;**50**:W159–64.
12. Moret N, Clark NA, Hafner M, Wang Y, Lounkine E, Medvedovic M, et al. Cheminformatics tools for analyzing and designing optimized small-molecule collections and libraries. *Cell Chem Biol* 2019;**26**:765–777.e3.
13. Scheele C, Nielsen AR, Walden TB, Sewell DA, Fischer CP, Brogan RJ, et al. Altered regulation of the PINK1 locus: a link between type 2 diabetes and neurodegeneration?. *FASEB J* 2007;**21**:3653–65.
14. Kupersmidt I, Su QJ, Grewal A, Sundaresh S, Halperin I, Flynn J, et al. Ontology-based meta-analysis of global collections of high-throughput public data. *PLoS One* 2010;**5**:e13066.
15. Chen EY, Tan CM, Kou Y, Duan Q, Wang Z, Meirelles GV, et al. Enrichr: interactive and collaborative HTML5 gene list enrichment analysis tool. *BMC Bioinformatics* 2013;**14**:128.
16. Luo L, Liu M. Adipose tissue in control of metabolism. *J Endocrinol* 2016;**231**:R77–99.
17. Shin JM, Kim N. Pharmacokinetics and pharmacodynamics of the proton pump inhibitors. *J Neurogastroenterol Motil* 2013;**19**:25–35.
18. Roberts S, Narisawa S, Harney D, Millán JL, Farquharson C. Functional involvement of PHOSPHO1 in matrix vesicle-mediated skeletal mineralization. *J Bone Miner Res* 2007;**22**:617–27.
19. Staines KA, Myers K, Little K, Ralston SH, Farquharson C. Proton pump inhibitors inhibit PHOSPHO1 activity and matrix mineralisation *in vitro*. *Calcif Tissue Int* 2021;**109**:696–705.
20. Jumper J, Evans R, Pritzel A, Green T, Figurnov M, Ronneberger O, et al. Highly accurate protein structure prediction with AlphaFold. *Nature* 2021;**596**:583–9.
21. Chen S, Li Z, Zhang S, Zhou Y, Xiao X, Cui P, et al. Emerging biotechnology applications in natural product and synthetic pharmaceutical analyses. *Acta Pharm Sin B* 2022;**12**:4075–97.
22. Roberts SJ, Stewart AJ, Schmid R, Blindauer CA, Bond SR, Sadler PJ, et al. Probing the substrate specificities of human PHOSPHO1 and PHOSPHO2. *Biochim Biophys Acta* 2005;**1752**:73–82.
23. Boon MR, Kooijman S, van Dam AD, Pelgrom LR, Berbée JF, Visseren CA, et al. Peripheral cannabinoid 1 receptor blockade activates brown adipose tissue and diminishes dyslipidemia and obesity. *FASEB J* 2014;**28**:5361–75.
24. Perwitz N, Wenzel J, Wagner I, Büning J, Drenckhan M, Zarse K, et al. Cannabinoid type 1 receptor blockade induces trans-differentiation towards a brown fat phenotype in white adipocytes. *Diabetes Obes Metab* 2010;**12**:158–66.
25. Hao S, Sun J, Tian X, Sun X, Zhang Z, Gao Y. Lansoprazole enhances the antidiabetic effect of sitagliptin in mice with diet-induced obesity and healthy human subjects. *J Pharm Pharmacol* 2014;**66**:1133–9.
26. Benchamana A, Mori H, MacDougald OA, Soodvilai S. Regulation of adipocyte differentiation and metabolism by lansoprazole. *Life Sci* 2019;**239**:116897.
27. Lu J, Shang X, Yao B, Sun D, Liu J, Zhang Y, et al. The role of CYP1A1/2 in cholesterol ester accumulation provides a new perspective for the treatment of hypercholesterolemia. *Acta Pharm Sin B* 2023;**13**:648–61.
28. Bödvarsdóttir TB, Hove KD, Gotfredsen CF, Pridal L, Vaag A, Karlsten AE, et al. Treatment with a proton pump inhibitor improves glycaemic control in Psammomys obesus, a model of type 2 diabetes. *Diabetologia* 2010;**53**:2220–3.
29. Gamil NM, Abd El Fattah MA, Ahmed MAE, Maklad YA, Gamal El Din AA, Eid NI. Lansoprazole enhances the antidiabetic effect of dapagliflozin in fortified diet-fed streptozotocin-treated diabetic rats. *J Biochem Mol Toxicol* 2020;**34**:e22451.
30. Lin MH, Wu WT, Chen YC, Lin TK, Chou YC, Sun CA. Association between clinical use of lansoprazole and the risk of type 2 diabetes mellitus: a pharmacoepidemiological cohort study. *Diabetol Metab Syndr* 2023;**15**:96.
31. Reddy R, Dayal D, Sachdeva N, Attri SV, Gupta VK. Combination therapy with lansoprazole and cholecalciferol is associated with a slower decline in residual beta-cell function and lower insulin requirements in children with recent onset type 1 diabetes: results of a pilot study. *Einstein (Sao Paulo)* 2022;**20**:eAO0149.
32. Liu Y, Wu Y, Jiang M. The emerging roles of PHOSPHO1 and its regulated phospholipid homeostasis in metabolic disorders. *Front Physiol* 2022;**13**:935195.
33. Gliniak CM, Scherer PE. PHOSPHO1 puts the breaks on thermogenesis in brown adipocytes. *Proc Natl Acad Sci U S A* 2020;**117**:16726–8.
34. Shin JM, Munson K, Vagin O, Sachs G. The gastric HK-ATPase: structure, function, and inhibition. *Pflugers Arch* 2009;**457**:609–22.
35. Thomson AB, Sauve MD, Kassam N, Kamitakahara H. Safety of the long-term use of proton pump inhibitors. *World J Gastroenterol* 2010;**16**:2323–30.